Inversion of normal moveout for monoclinic media

Vladimir Grechka[†], Pedro Contreras[⋆], and Ilya Tsvankin[†]

[†]Center for Wave Phenomena, Department of Geophysics,

Colorado School of Mines, Golden, CO 80401-1887

[⋆]PDVSA-INTEVEP, Apartado 76343, Caracas 1070A, Venezuela

ABSTRACT

Multiple vertical fracture sets, possibly combined with horizontal fine layering, produce an equivalent medium of monoclinic symmetry with a horizontal symmetry plane. Although monoclinic models may be rather common for fractured formations, they have been hardly used in seismic methods of fracture detection due to the large number of independent elements in the stiffness tensor. Here, we show that multi-component wide-azimuth reflection data (combined with known vertical velocity or reflector depth) or multi-azimuth walkaway VSP surveys provide enough information to invert for all but one anisotropic parameters of monoclinic media.

To facilitate the inversion procedure, we introduce a Thomsen-style parameterization for monoclinic media that includes the vertical velocities of the P-wave and one of the split S-waves and a set of dimensionless anisotropic coefficients. Our notation, defined for the coordinate frame associated with the polarization directions of the vertically propagating shear waves, captures the combinations of the stiffnesses responsible for the normal-moveout (NMO) ellipses of all three pure modes. The first group of the anisotropic parameters contains seven coefficients ($\epsilon^{(1,2)}$, $\delta^{(1,2,3)}$, and $\gamma^{(1,2)}$) analogous to those defined by Tsvankin for the higher-symmetry orthorhombic model. The parameters $\epsilon^{(1,2)}$, $\delta^{(1,2)}$, and $\gamma^{(1,2)}$ are primarily responsible for the pure-mode NMO velocities along the coordinate axes x_1 and x_2 (i.e., in the shear-wave polarization directions). The remaining coefficient, $\delta^{(3)}$, is not constrained by conventional-spread reflection traveltimes in a horizontal monoclinic layer. The second parameter group consists of the newly introduced coefficients $\zeta^{(1,2,3)}$ which control the *rotation* of the P, S_1, and S_2 NMO ellipses with respect to the horizontal coordinate axes. Misalignment of the P-wave NMO ellipse and shear-wave polarization directions was recently observed on field data by Pérez et al.

Our parameter-estimation algorithm, based on NMO equations valid for any strength of the anisotropy, is designed to obtain anisotropic parameters of mono-

clinic media by inverting the vertical velocities and NMO ellipses of the waves P, S_1 and S_2. A Dix-type representation of the NMO velocity of mode-converted waves makes it possible to replace the pure shear modes in reflection surveys with the waves PS_1 and PS_2. Numerical tests show that our method yields stable estimates of all relevant parameters for both a single layer and a horizontally stratified monoclinic medium.

Keywords.—seismic anisotropy, seismic inversion, reflection moveout, multicomponent seismic

INTRODUCTION

Natural fractures usually occur in vertical or subvertical sets (networks), which makes fractured reservoirs azimuthally anisotropic with respect to elastic wave propagation. The simplest azimuthally anisotropic model, transverse isotropy with a horizontal symmetry axis (HTI), describes a formation with a single set of parallel, vertical, rotationally invariant fractures embedded in a purely isotropic background matrix. Making this physical model more complicated inevitably leads to media of lower symmetry, such as orthorhombic, monoclinic, or triclinic. For example, the addition of another identical system of vertical cracks or the presence of transverse isotropy with a vertical symmetry axis (VTI) in the matrix (e.g., due to fine layering) makes the effective medium orthorhombic. If a formation contains two different non-orthogonal systems of vertical fractures in an isotropic or VTI background, the medium becomes monoclinic with a horizontal symmetry plane. (In the special case of two orthogonal vertical fracture sets the model has the orthorhombic symmetry.) Three or more sets of vertical fractures generally make the effective medium monoclinic; only if the normal and shear compliances for all sets are identical, the medium is orthorhombic (Sayers, 1998).

Potential importance of monoclinic models in seismic reservoir characterization is corroborated by abundant geological (in-situ) evidence of multiple vertical fracture sets (e.g., Schoenberg and Sayers 1995). Note that if the background medium does not have a horizontal plane of symmetry, a vertical fracture set may produce a monoclinic medium with a *vertical* or dipping symmetry plane. A model of this kind, for example, was inferred by Winterstein and Meadows (1991) from multi-azimuth walkaway VSP measurements of shear-wave polarization over a fractured formation. Here, however, we restrict ourselves to the more simple (from the standpoint of reflection seismic) monoclinic media with a horizontal symmetry plane.

Although the general theory of seismic wave propagation in monoclinic and even

triclinic media is well known (e.g., Fedorov 1968; Musgrave 1970), velocity analysis and parameter estimation for monoclinic media is a highly challenging task. Due to the large number of stiffness coefficients (13) describing monoclinic media with a known orientation of the symmetry plane, "blind" inversion of seismic signatures is expected to be non-unique and suffer from trade-offs between the stiffnesses. To avoid this ambiguity and focus the inversion procedure on the "extractable" parameters, we follow the idea originally proposed for VTI media by Thomsen (1986) and attempt to identify the combinations of the stiffness coefficients responsible for seismic signatures commonly measured from reflection data. Since moveout velocity analysis is one of the most reliable tools for mapping the elastic properties of the subsurface, we use normal-moveout (NMO) velocities of P- and S-waves from a horizontal reflector to define the anisotropic parameters of monoclinic media. A subset of these parameters coincides with the Thomsen-style anisotropic coefficients introduced by Tsvankin (1997) for orthorhombic media. The remaining parameters can be related to the dimensionless anisotropic coefficients defined by Mensch and Rasolofosaon (1997) and Pšenčík and Gajewski (1998) for arbitrary anisotropic media. Our notation, however, is somewhat different because it is designed to simplify the moveout equations, while the alternative parameterizations are derived from an approximate phase-velocity function.

To recover the anisotropic parameters from reflection data, we use analytic expressions for azimuthally varying NMO velocities of P- and S-waves. The moveout-based approach to anisotropic parameter estimation was first developed for P-waves in VTI media by Alkhalifah and Tsvankin (1995). They showed that the dip-direction P-wave NMO velocity in vertically inhomogeneous VTI media is controlled by just two combinations of medium parameters – the NMO velocity from a horizontal reflector $V_{\rm nmo}(0)$ and the "anellipticity" coefficient η; both $V_{\rm nmo}(0)$ and η can be obtained from P-wave reflection traveltimes alone.

Moveout inversion in azimuthally anisotropic media requires analysis of the az-

imuthal dependence of reflection traveltimes and has to be performed in 3-D geometry. Grechka and Tsvankin (1998a) proved that the azimuthal variation of NMO velocity of pure modes generally represents an *ellipse*, even in arbitrary anisotropic, heterogeneous media. NMO ellipses of reflection events can be found by applying semblance velocity analysis to 3-D data acquired either in wide-azimuth surveys or on at least three 2-D lines with sufficiently different azimuths (Corrigan et al. 1996; Grechka, Tsvankin and Cohen 1999).

For vertical transverse isotropy, the P-wave NMO ellipse (and, therefore, NMO velocity measured in *any* direction with respect to the dip plane of the reflector) is still governed by the two Alkhalifah-Tsvankin parameters ($V_{\rm nmo}(0)$ and η) and cannot be inverted for the vertical velocity (Grechka and Tsvankin 1998a). However, if the symmetry axis of a TI medium is tilted by a sufficiently large angle (at least 30°) from the vertical, P-wave NMO ellipses from horizontal and dipping reflectors provide enough information to determine the P-wave velocity in the symmetry direction, Thomsen's (1986) coefficients ϵ and δ, and the tilt and azimuth of the symmetry axis (Grechka and Tsvankin 1998b). Thus, in contrast to VTI media, for the TI model with a tilted symmetry axis surface seismic data can be used to build anisotropic velocity models in *depth*.

Unfortunately, for lower-symmetry orthorhombic and monoclinic models P-wave reflection moveout does not constrain the vertical velocity and reflector depth. The inversion of P-wave NMO ellipses in orthorhombic media with a horizontal symmetry plane was discussed by Grechka and Tsvankin (1999a). The NMO velocity of horizontal and dipping events in an orthorhombic layer is governed by six parameters: the azimuth of one of the vertical symmetry planes, two zero-dip symmetry-plane NMO velocities $V_{\rm nmo}^{(1,2)}$, and three "anellipticity" coefficients $\eta^{(1,2,3)}$ analogous to the Alkhalifah-Tsvankin coefficient η. Additional information about the parameters of orthorhombic media can be obtained from moveout of shear or converted waves. Grechka, Theophanis and Tsvankin (1999) demonstrated that combining the NMO

ellipses of P- and two split PS-waves (PS_1 and PS_2) makes it possible to find the azimuths of the vertical symmetry planes and eight (out of nine) elastic constants, provided the reflector depth is known.

Here, we devise a parameter-estimation procedure for horizontally layered monoclinic media based on the NMO ellipses and vertical velocities of the P-wave and two split shear waves. Despite the absence of vertical symmetry planes in our model, the polarization directions of the vertically propagating shear waves establish a natural coordinate frame with the vanishing stiffness coefficient c_{45}. We specify the anisotropic parameters in this coordinate frame (where the stiffness tensor has 12 independent elements) by analogy with the Thomsen-style notation of Tsvankin (1997) for orthorhombic media. In contrast to orthorhombic media, however, the NMO ellipses of the three pure reflection modes in general monoclinic media have different orientations. Hence, moveout data yield three more equations than in orthorhombic media, which can be inverted for three additional parameters responsible for the rotation angles of the NMO ellipses. On the whole, the vertical velocities and NMO ellipses of P- and two split S-waves can be used to estimate eleven (out of twelve) parameters of monoclinic media. We present numerical tests for a single layer and stratified monoclinic media with substantial anisotropy to confirm the accuracy of our inversion procedure and its stability with respect to errors in the input data.

STIFFNESS TENSOR IN MONOCLINIC MEDIA

The density-normalized elastic stiffness tensor $c_{ijk\ell}$ in a monoclinic medium with a horizontal symmetry plane $[x_1, x_2]$ can be represented in the two-index notation as follows (e.g., Musgrave 1970):

$$\mathbf{c}^{(\mathrm{mnc})} = \begin{pmatrix} c_{11} & c_{12} & c_{13} & 0 & 0 & c_{16} \\ c_{12} & c_{22} & c_{23} & 0 & 0 & c_{26} \\ c_{13} & c_{23} & c_{33} & 0 & 0 & c_{36} \\ 0 & 0 & 0 & c_{44} & c_{45} & 0 \\ 0 & 0 & 0 & c_{45} & c_{55} & 0 \\ c_{16} & c_{26} & c_{36} & 0 & 0 & c_{66} \end{pmatrix} . \tag{1}$$

$\mathbf{c}^{(\mathrm{mnc})}$ has four additional non-zero components (c_{16}, c_{26}, c_{36}, and c_{45}) compared to the stiffness tensors for VTI, HTI, and orthorhombic media. Note that the tensor $\mathbf{c}^{(\mathrm{mnc})}$ is supposed to be defined in a certain coordinate frame that is not completely specified yet. While the vertical axis x_3 is fixed in the direction orthogonal to the symmetry plane, the axes x_1 and x_2 can be rotated in an arbitrary fashion. Rotating the tensor $\mathbf{c}^{(\mathrm{mnc})}$ around the x_3-axis leads to another tensor $\tilde{\mathbf{c}}^{(\mathrm{mnc})}$ with the same vanishing components and different values of the non-zero components (Appendix A).

For the purpose of parameter estimation, it is important to choose a coordinate frame where the mathematical description of seismic wave propagation has the simplest possible form. Kinematic and polarization properties of seismic waves in anisotropic media can be derived from the Christoffel equation (e.g., Musgrave 1970):

$$F \equiv [G_{i\ell} - \delta_{i\ell}]\, U_\ell = 0\,, \tag{2}$$

where $\mathbf{U}$ is the unit polarization vector of a plane wave, $\delta_{i\ell}$ is the Kronecker's symbolic δ, and $\mathbf{G}$ is the symmetric Christoffel matrix; summation over repeated indexes (from 1 to 3) is implied. The elements of $\mathbf{G}$ are given by

$$G_{i\ell} = c_{ijk\ell}\, p_j p_k\,, \tag{3}$$

where $\mathbf{p}$ is the slowness vector.

As discussed in Appendix A, for a certain rotation angle of the horizontal axes

$$c_{45} = 0\,. \tag{4}$$

In this case, in addition to the reduction in the number of stiffnesses, the matrix $\mathbf{G}$ becomes diagonal for vertical propagation (i.e., for waves with the slowness vector $\mathbf{p} = \{0, 0, p_3\}$). As a result, for the coordinate system with $c_{45} = 0$ the horizontal axes x_1 and x_2 coincide with the polarization directions of the vertically traveling shear waves. Denoting the fast shear wave by S_1 and the slow one by S_2, we can write the vertical slowness components $q \equiv p_3$ for waves propagating in the x_3-direction as (Appendix A)

$$\begin{aligned} q^P &= \frac{1}{\sqrt{c_{33}}}\,, \\ q^{S_1} &= \frac{1}{\sqrt{c_{55}}}\,, \\ q^{S_2} &= \frac{1}{\sqrt{c_{44}}}\,. \end{aligned} \tag{5}$$

Here it is assumed that the x_1-axis points in the direction of the polarization of the fast shear wave S_1, which implies that

$$c_{55} > c_{44}\,. \tag{6}$$

The polarization vectors of the vertically propagating waves in this coordinate system can be written as

$$\begin{aligned} \mathbf{U}^{S_1}(q^{S_1}) &= \{1, 0, 0\}\,, \\ \mathbf{U}^{S_2}(q^{S_2}) &= \{0, 1, 0\}\,, \\ \mathbf{U}^{P}(q^{P}) &= \{0, 0, 1\}\,. \end{aligned} \tag{7}$$

Equations (7) formally define the coordinate frame that will be used throughout the paper. The corresponding stiffness coefficients are specified by equations (1), (4), and inequality (6).

NMO ELLIPSES FOR HORIZONTAL REFLECTORS

Normal-moveout velocity, analytically defined in the zero-spread limit, describes the hyperbolic portion of reflection moveout. Grechka and Tsvankin (1998a) showed that azimuthally varying NMO velocity $V_{\rm nmo}(\alpha)$ of pure (non-converted) modes is represented by the following quadratic form that usually specifies an *ellipse* in the horizontal plane:

$$V_{\rm nmo}^{-2}(\alpha) = W_{11}\cos^2\alpha + 2\,W_{12}\sin\alpha\cos\alpha + W_{22}\sin^2\alpha\,, \tag{8}$$

where $\mathbf{W}$ is a symmetric matrix,

$$W_{ij} = \tau_0\,\frac{\partial^2\tau}{\partial x_i \partial x_j}\bigg|_{\mathbf{x}_{\rm CMP}} = \tau_0\,\frac{\partial p_i}{\partial x_j}\bigg|_{\mathbf{x}_{\rm CMP}}\,, \qquad (i,j=1,2)\,. \tag{9}$$

Here, $\tau(x_1,\,x_2)$ is the one-way traveltime from the zero-offset reflection point to the location $\mathbf{x}\,\{x_1,\,x_2\}$ at the surface, τ_0 is the one-way zero-offset traveltime, p_i are the components of the slowness vector corresponding to the ray recorded at the point $\mathbf{x}$, and $\mathbf{x}_{\rm CMP}$ is the common-midpoint (CMP) location. Equation (8) holds for arbitrary anisotropic, heterogeneous media provided the traveltime can be expanded in a Taylor series in the horizontal coordinates.

Equivalently, the NMO ellipse (8) can be written through the eigenvalues $\lambda_{1,2}$ of the matrix $\mathbf{W}$ as (Grechka and Tsvankin 1998a)

$$V_{\rm nmo}^{-2}(\alpha) = \lambda_1\cos^2(\alpha-\beta) + \lambda_2\sin^2(\alpha-\beta)\,, \tag{10}$$

where

$$\lambda_{1,2} = \frac{1}{2}\left[W_{11}+W_{22} \pm \sqrt{(W_{11}-W_{22})^2+4W_{12}^2}\right]\,, \tag{11}$$

and β is the rotation angle of the ellipse with respect to the coordinate axes,

$$\tan 2\beta = \frac{2\,W_{12}}{W_{11}-W_{22}}\,. \tag{12}$$

If $W_{12} = 0$, the axes of the ellipse are aligned with the coordinate directions. Both the numerator and denominator of equation (12) can go to zero only if $\lambda_1 = \lambda_2$, which means that the ellipse degenerates into a circle.

The values of the semi-major and semi-minor axes of the ellipse are $1/\sqrt{\lambda_1}$ and $1/\sqrt{\lambda_2}$. In the uncommon case of negative λ_1 or λ_2, the squared NMO velocity for at least some azimuths is negative as well, and equations (8) and (10) no longer describe an ellipse.

To find the matrix $\mathbf{W}$ from equation (9) and then the normal-moveout velocity from equation (8), we need to determine the spatial derivatives of the one-way traveltime. For the model of a single homogeneous anisotropic layer with arbitrary symmetry, $\mathbf{W}$ can be found explicitly as a function of the slowness vector (Grechka, Tsvankin and Cohen 1999). If the reflector is horizontal,

$$\mathbf{W} = \frac{-q}{q_{,11}q_{,22} - q_{,12}^2} \begin{pmatrix} q_{,22} & -q_{,12} \\ -q_{,12} & q_{,11} \end{pmatrix}, \tag{13}$$

where $q \equiv q(p_1, p_2) \equiv p_3$ is the vertical component of the slowness vector, p_1 and p_2 are the horizontal slownesses, and $q_{,ij} \equiv \partial^2 q / \partial p_i \partial p_j$; equation (13) is evaluated for the zero-offset ray ($p_1 = p_2 = 0$).

The matrix $\mathbf{W}$ for horizontal events in monoclinic media is obtained from equation (13) by substituting the corresponding values of q [equations (5)] and the derivatives $q_{,i}$ and $q_{,ij}$ which can be determined from the Christoffel equation (2). The exact expressions for the matrices $\mathbf{W}^P$, $\mathbf{W}^{S_1}$, and $\mathbf{W}^{S_2}$ describing NMO ellipses of all three waves in a monoclinic layer in terms of the stiffness coefficients c_{ij} are derived in Appendix B.

Equations (B-2)–(B-7) help to identify the stiffness coefficients (and their combinations) that influence the NMO ellipses. First, note that the coefficient c_{12} is not present in any of the equations (B-2)–(B-7) and, therefore, cannot be found from the NMO velocities of pure reflection modes in a horizontal monoclinic layer. The same conclusion regarding c_{12} was drawn by Grechka, Theophanis and Tsvankin (1999) for

a horizontal orthorhombic layer with a horizontal symmetry plane.

Second, the coefficients c_{16}, c_{26}, and c_{36}, which vanish in orthorhombic media, contribute to the diagonal elements W_{11}^Q and W_{22}^Q only through their products $c_{i6}c_{j6}$ $(i,j=1,2,3)$. Furthermore, the semi-axes of the NMO ellipses [equation (11)] do not contain terms linear in c_{i6} either. Therefore, approximations for $W_{\ell\ell}^Q$ and elliptical semi-axes linearized in the typically small stiffnesses c_{i6} should have the same form as the corresponding exact expressions in orthorhombic media. This is a strong indication that the parameterization introduced by Tsvankin (1997) for orthorhombic symmetry can also be useful for monoclinic models.

In contrast, the off-diagonal matrix elements W_{12}^Q are approximately *linear* in c_{i6}. Since the rotation angle β of the NMO ellipse is almost proportional to W_{12}^Q [equation (12)], the coefficients c_{i6} are primarily responsible for the deviation of the axes of the NMO ellipses from the polarization directions of the vertically propagating shear waves; this is discussed in more detail in the next section.

ANISOTROPIC PARAMETERS OF MONOCLINIC MEDIA AND LINEARIZED NMO ELLIPSES

Notation for monoclinic media

Analysis of the expressions for the NMO ellipses helped us to develop a convenient parameterization for monoclinic media by generalizing Tsvankin's (1997) notation for orthorhombic symmetry. Expressions for these parameters in terms of the density-normalized stiffness coefficients are given below. It should be emphasized that the horizontal coordinate axes are aligned with the polarization directions of the vertically traveling shear waves.

- V_{P0} – the P-wave vertical velocity:

$$V_{P0} \equiv \sqrt{c_{33}}\,. \tag{14}$$

- V_{S0} – the vertical velocity of the fast shear wave S_1 polarized in the x_1-direction:

$$V_{S0} \equiv \sqrt{c_{55}}\,. \tag{15}$$

- $\epsilon^{(1)}$ – the parameter defined analogously to the VTI coefficient ϵ in the $[x_2, x_3]$-plane (the superscript denotes the axis x_1 orthogonal to the $[x_2, x_3]$-plane):

$$\epsilon^{(1)} \equiv \frac{c_{22} - c_{33}}{2\,c_{33}}\,. \tag{16}$$

- $\delta^{(1)}$ – the parameter analogous to the VTI coefficient δ in the $[x_2, x_3]$-plane:

$$\delta^{(1)} \equiv \frac{(c_{23} + c_{44})^2 - (c_{33} - c_{44})^2}{2\,c_{33}\,(c_{33} - c_{44})}\,. \tag{17}$$

- $\gamma^{(1)}$ – the parameter analogous to the VTI coefficient γ in the $[x_2, x_3]$-plane:

$$\gamma^{(1)} \equiv \frac{c_{66} - c_{55}}{2\,c_{55}}\,. \tag{18}$$

- $\epsilon^{(2)}$ – the parameter analogous to the VTI coefficient ϵ in the $[x_1, x_3]$-plane:

$$\epsilon^{(2)} \equiv \frac{c_{11} - c_{33}}{2\,c_{33}}\,. \tag{19}$$

- $\delta^{(2)}$ – the parameter analogous to the VTI coefficient δ in the $[x_1, x_3]$-plane:

$$\delta^{(2)} \equiv \frac{(c_{13} + c_{55})^2 - (c_{33} - c_{55})^2}{2\,c_{33}\,(c_{33} - c_{55})}\,. \tag{20}$$

- $\gamma^{(2)}$ – the parameter analogous to the VTI coefficient γ in the $[x_1, x_3]$-plane:

$$\gamma^{(2)} \equiv \frac{c_{66} - c_{44}}{2\,c_{44}}\,. \tag{21}$$

- $\delta^{(3)}$ – the parameter analogous to the VTI coefficient δ in the $[x_1, x_2]$-plane:

$$\delta^{(3)} \equiv \frac{(c_{12} + c_{66})^2 - (c_{11} - c_{66})^2}{2\,c_{11}\,(c_{11} - c_{66})}\,. \tag{22}$$

- $\zeta^{(1)}$ – the parameter responsible for the rotation of S_1-wave NMO ellipse:

$$\zeta^{(1)} \equiv \frac{c_{16} - c_{36}}{2\, c_{33}}\,. \tag{23}$$

- $\zeta^{(2)}$ – the parameter responsible for the rotation of S_2-wave NMO ellipse:

$$\zeta^{(2)} \equiv \frac{c_{26} - c_{36}}{2\, c_{33}}\,. \tag{24}$$

- $\zeta^{(3)}$ – the parameter responsible for the rotation of P-wave NMO ellipse:

$$\zeta^{(3)} \equiv \frac{c_{36}}{c_{33}}\,. \tag{25}$$

The vertical velocities and anisotropic coefficients $\epsilon^{(i)}$, $\delta^{(i)}$ and $\gamma^{(i)}$ are defined exactly in the same way as the corresponding Tsvankin's (1997) parameters for orthorhombic media. One of the advantages of Tsvankin's notation is the possibility of extending the VTI equations for velocity and polarization to the vertical symmetry planes of orthorhombic media by simply replacing Thomsen's VTI parameters with the appropriate set of the coefficients $\epsilon^{(i)}$, $\delta^{(i)}$ and $\gamma^{(i)}$. Unfortunately, the monoclinic model does not have vertical symmetry planes, and the VTI substitution is no longer valid. Still, the "orthorhombic" coefficients proved useful in simplifying the NMO equations in a monoclinic layer.

The parameters $\zeta^{(1,2,3)}$ depend on the purely "monoclinic" stiffness elements that vanish in orthorhombic media. The coefficient $\zeta^{(3)}$ becomes identical to the anisotropic parameter χ_z introduced by Mensch and Rasolofosaon (1997) if the reference velocity in their model is equal to $\sqrt{c_{33}}$ and the coordinate axes x_1 and x_2 are rotated in such a way that the stiffness coefficient $c_{45} = 0$. The parameters $\zeta^{(1)}$ and $\zeta^{(2)}$ are different from their counterparts in Mensch–Rasolofosaon (1997) notation because the latter is based on the weak-anisotropy approximation for phase velocity.

Approximations for NMO ellipses

To demonstrate that the anisotropic coefficients defined above are useful in describing the NMO ellipses in monoclinic media, we linearize the exact equations (B-2)–(B-7) in terms of $\zeta^{(1)}$, $\zeta^{(2)}$, and $\zeta^{(3)}$. Also, additional linearizations in the parameters $\epsilon^{(1,2)}$ $\delta^{(1,2)}$ and $\gamma^{(1,2)}$ were performed for the elements W_{12}^{Q} of all matrices $\mathbf{W}^{Q}$ (but not for W_{11}^{Q} and W_{22}^{Q}). This yields the following approximate expressions for the NMO ellipses in a monoclinic layer:

$$W_{11}^{P} = \frac{1}{V_{P0}^2\,(1+2\,\delta^{(2)})}\,, \qquad W_{12}^{P} = -2\,\frac{\zeta^{(3)}}{V_{P0}^2}\,, \qquad W_{22}^{P} = \frac{1}{V_{P0}^2\,(1+2\,\delta^{(1)})}\,; \tag{26}$$

$$W_{11}^{S_1} = \frac{1}{V_{S_1}^2\,(1+2\,\sigma^{(2)})}\,, \quad W_{12}^{S_1} = -2\,\frac{\zeta^{(1)}}{V_{S_1}^2}\,\left(\frac{V_{P0}}{V_{S_1}}\right)^2\,, \quad W_{22}^{S_1} = \frac{1}{V_{S_1}^2\,(1+2\,\gamma^{(1)})}\,; \tag{27}$$

$$W_{11}^{S_2} = \frac{1}{V_{S_2}^2\,(1+2\,\gamma^{(2)})}\,, \quad W_{12}^{S_2} = -2\,\frac{\zeta^{(2)}}{V_{S_2}^2}\,\left(\frac{V_{P0}}{V_{S_2}}\right)^2\,, \quad W_{22}^{S_2} = \frac{1}{V_{S_2}^2\,(1+2\,\sigma^{(1)})}\,. \tag{28}$$

Here

$$\sigma^{(2)} \equiv \left(\frac{V_{P0}}{V_{S_1}}\right)^2\,\left(\epsilon^{(2)}-\delta^{(2)}\right)\,, \qquad \sigma^{(1)} \equiv \left(\frac{V_{P0}}{V_{S_2}}\right)^2\,\left(\epsilon^{(1)}-\delta^{(1)}\right)\,, \tag{29}$$

$$V_{S_1} \equiv V_{S0}\,, \qquad V_{S_2} \equiv V_{S0}\,\sqrt{\frac{1+2\,\gamma^{(1)}}{1+2\,\gamma^{(2)}}}\,; \tag{30}$$

V_{S_1} and V_{S_2} are the vertical velocities of the fast and slow shear waves, respectively.

It is interesting that the approximate diagonal elements W_{11}^{Q} and W_{22}^{Q} in equations (26)–(28) are identical to the corresponding *exact* expressions for orthorhombic media given in Grechka, Theophanis and Tsvankin (1999). As mentioned above, the "monoclinic" coefficients $\zeta^{(1,2,3)}$ contribute to W_{11}^{Q} and W_{22}^{Q} only through their products which were dropped during the linearization procedure.

In contrast, the off-diagonal matrix elements W_{12}^{Q} in equations (26)–(28) are linear in the coefficients $\zeta^{(1,2,3)}$ and quadratic in the other anisotropic parameters. If we

make the medium orthorhombic by setting $\zeta^{(1,2,3)} = 0$, the elements W_{12}^Q vanish, which means that the NMO ellipses of all three modes are aligned with the axes x_1 and x_2 [see equation (12)]. In this case, the diagonal elements W_{11}^Q and W_{22}^Q determine the normal-moveout velocities in the symmetry planes of orthorhombic media (i.e., the semi-axes of the NMO ellipses).

For monoclinic media, in general all three $W_{12}^Q \neq 0$, and the axes of the NMO ellipses of the P-, S_1- and S_2-waves deviate from the coordinate directions (i.e., from the S-wave polarization vectors) and have different orientations. Sayers (1998) drew similar conclusions from his study of the principal azimuthal directions of the P-wave phase-velocity function in monoclinic media. Experimental evidence of the misalignment of the P-wave NMO ellipse and shear-wave polarization directions was presented by Pérez, Grechka and Michelena (1999) who analyzed multicomponent data acquired over a fractured carbonate reservoir.

Numerical tests show that the accuracy of the approximations (26)–(28) depends mostly on the parameters $\zeta^{(1,2,3)}$ and is less sensitive to the other anisotropic coefficients. As follows from the results of Bakulin, Grechka and Tsvankin (1999), for the simplest (and probably most common) monoclinic models due to two non-orthogonal vertical fracture sets, the absolute values of $\zeta^{(1,2,3)}$ are usually limited by 0.05-0.06. The example in Fig. 1 demonstrates that for such small values of $\zeta^{(1,2,3)}$ equations (26)–(28) (dotted lines) yield a qualitatively adequate approximation for the exact NMO ellipses (solid) computed from equations (B-2)–(B-7). The error of the weak-anisotropy approximation, however, rapidly increases if the absolute values of the parameters ζ reach 0.08–0.1.

As predicted by equations (26)–(28), the axes of the NMO ellipses of P-, S_1-, and S_2-waves in Fig. 1 are parallel neither to each other nor to the coordinate directions. The azimuths of their semi-major axes with respect to the polarization vector of the fast S-wave (azimuth 0° in Fig. 1) are $\beta^P = 32°$, $\beta^{S_1} = 349°$, and $\beta^{S_2} = 106°$. The

difference in the orientations of the NMO ellipses is a distinctive feature of monoclinic media that can be used in the inversion for the anisotropic parameters.

PARAMETER ESTIMATION

Analysis of the weak-anisotropy approximation

Although equations (26)–(28) lose accuracy with increasing $|\zeta^{(1,2,3)}|$, they provide a useful insight into the influence of the medium parameters on normal moveout and help to design the inversion procedure. Just one of the anisotropic coefficients, $\delta^{(3)}$, is not contained in any of these equations and, therefore, cannot be estimated from NMO velocities of horizontal events. Since $\delta^{(3)}$ is the only parameter that contains the stiffness element c_{12}, this result is consistent with our earlier observation that c_{12} does not contribute to the exact NMO ellipses [equations (B-2)–(B-7)].

The diagonal elements W_{11}^Q and W_{22}^Q of the matrices $\mathbf{W}^Q$ in equations (26)–(28) yield the NMO velocities along the x_1- and x_2-axes (i.e., in the polarization directions of the vertically propagating shear waves). As mentioned above, W_{11}^Q and W_{22}^Q do not contain terms linear in the "monoclinic" coefficients $\zeta^{(1,2,3)}$; the same is true for the semi-axes of the NMO ellipses $1/\sqrt{\lambda_\ell^Q}$.

Neglecting the contributions of the ζ coefficients to the diagonal elements of the NMO ellipses makes the inversion of W_{11}^Q and W_{22}^Q completely analogous to the parameter-estimation problem in orthorhombic media discussed by Grechka, Theophanis and Tsvankin (1999). As in orthorhombic media, the elements $W_{\ell\ell}^Q$ for the three waves (or the semi-axes of the ellipses λ_ℓ^Q) provide us with *five* equations for the unknown parameters. Although there seems to be a total of six equations, the elements $W_{22}^{S_1}$ and $W_{11}^{S_2}$ in equations (26)–(28) are equal to each other. (This follows from the relations (30) between the vertical shear-wave velocities and the anisotropic parameters $\gamma^{(1)}$ and $\gamma^{(2)}$.) In combination with the vertical velocities V_{P0}, V_{S_1} and

V_{S_2}, the semi-axes of the NMO ellipses provide us with eight equations for eight unknown parameters – the velocities V_{P0}, $V_{S0} = V_{S_1}$, and six anisotropic coefficients $\epsilon^{(1,2)}$, $\delta^{(1,2)}$ and $\gamma^{(1,2)}$. Feasibility of this inversion procedure for orthorhombic media has been proved by Grechka, Theophanis and Tsvankin (1999) who developed an inversion algorithm based on moveout velocities of P- and PS-waves and successfully tested it on physical-modeling data.

The three remaining anisotropic coefficients of monoclinic media ($\zeta^{(1,2,3)}$) can be estimated from the off-diagonal matrix elements W_{12}^Q, which yield three linear (in the weak-anisotropy approximation) equations for the three unknowns. Essentially, we infer the parameters ζ from the rotation angles β^Q of the NMO ellipses because β^Q are approximately proportional to W_{12}^Q [equation (12)]. Only if the elongation of the NMO ellipses is small (i.e., the ellipses are close to circles), the rotation angles β^Q are poorly constrained by the data. In this case, however, the elements W_{12}^Q (and the coefficients $\zeta^{(1,2,3)}$) have a more substantial influence on the elliptical semi-axes. As follows from equation (11), for quasi-circular ellipses with the eigenvalues $\lambda_1^Q \approx \lambda_2^Q$, the diagonal elements W_{11}^Q and W_{22}^Q are close to each other, which increases the contribution of W_{12}^Q to $\lambda_{1,2}^Q$.

Hence, the vertical velocities and NMO ellipses of the waves P, S_1 and S_2 contain enough information for moveout inversion in monoclinic media. Below, we confirm this conclusion by performing numerical inversion based on the exact NMO equations.

Numerical inversion in a single monoclinic layer

Input data for the parameter-estimation procedure include the vertical velocities and NMO ellipses of the three pure modes (P, S_1, S_2) determined from either wide-azimuth reflection data or walkaway VSP's. If the source does not generate shear waves, in reflection surveys they can be replaced with the converted modes PS_1 and PS_2. As shown by Grechka, Theophanis and Tsvankin (1999), azimuthally dependent

NMO velocities of converted waves in horizontally layered media with a horizontal symmetry plane are also described by the elliptical function (8). Furthermore, the generalized Dix equation discussed below leads to a simple relationship between the NMO ellipses of P-, S-, and PS-waves that can be used to obtain the NMO velocities of the pure shear reflections from P and PS data (Grechka, Theophanis and Tsvankin 1999).

The coordinate frame needed for moveout inversion can be established by performing Alford (1986) rotation of small-offset shear-wave data to identify the S-wave polarization directions at vertical incidence. Such a rotation is necessary anyway since the split shear or converted waves have to be separated prior to moveout analysis.

To invert the NMO ellipses for the medium parameters, we rewrite the exact NMO equations (B-2)–(B-7) in terms of the anisotropic coefficients defined by equations (14)–(25). Also, we represent the measured vertical shear-wave velocity V_{S2} through the γ coefficients using equation (30). Since the vertical velocities V_{P0} and $V_{S0} = V_{S1}$ are determined directly from the data, we need to invert the slow S-wave velocity V_{S2} and the NMO ellipses of the three pure modes for the vector of the anisotropic coefficients $\boldsymbol{\chi} \equiv [\epsilon^{(1)}, \epsilon^{(2)}, \delta^{(1)}, \delta^{(2)}, \gamma^{(1)}, \gamma^{(2)}, \zeta^{(1)}, \zeta^{(2)}, \zeta^{(3)}]$.

The inversion is performed by minimizing the following objective function:

$$\begin{aligned}\mathcal{F}(V_{P0}, V_{S0}, \boldsymbol{\chi}) \equiv & \left[\frac{\hat{V}_{P0}}{V_{P0}} - 1\right]^2 + \left[\frac{\hat{V}_{S_1}}{V_{S_1}} - 1\right]^2 + \left[\frac{\hat{V}_{S_2}}{V_{S_2}} - 1\right]^2 \\ & + \int_0^{2\pi} \left[\frac{\hat{V}^P_{\rm nmo}(\alpha)}{V^P_{\rm nmo}(\alpha)} - 1\right]^2 d\alpha + \int_0^{2\pi} \left[\frac{\hat{V}^{S_1}_{\rm nmo}(\alpha)}{V^{S_1}_{\rm nmo}(\alpha)} - 1\right]^2 d\alpha \\ & + \int_0^{2\pi} \left[\frac{\hat{V}^{S_2}_{\rm nmo}(\alpha)}{V^{S_2}_{\rm nmo}(\alpha)} - 1\right]^2 d\alpha\,, \end{aligned} \tag{31}$$

where the hats denote the measured quantities, while the quantities without hats are computed for a given set of medium parameters. The NMO velocities are obtained by substituting the exact equations (B-2)–(B-7) for the matrices $\mathbf{W}^Q$ into the equation (8) of the NMO ellipse. The measured vertical velocities V_{P0} and V_{S0} are included in the objective function to allow for adjustments in their values that may be needed

to better approximate the NMO ellipses in the presence of noise in input data. We search for a minimum of the objective function $\mathcal{F}$ using the simplex method (Press *et al.* 1987), with the initial values of the anisotropic coefficients determined from the weak anisotropy approximation [equations (26)–(28)].

Fig. 2 displays the inversion results for a monoclinic layer with the parameters specified in Fig. 1. The exact NMO velocities of the three modes were computed for azimuths 0°, 45°, 90°, and 135° from equations (B-2)–(B-7) and (8). To simulate errors in measured data, we added Gaussian noise with a variance of 2% to the vertical and NMO velocities. Then we reconstructed the NMO ellipses for each realization of the data (distorted by noise) and carried out the inversion based on the objective function (31).

The inversion procedure was repeated 200 times for different realizations of the Gaussian noise to examine the stability of the parameter estimation. The error bars in Fig. 2 correspond to ± the standard deviation and represent the 95% confidence intervals for each anisotropic parameter. Overall, the stability of the inversion algorithm is quite satisfactory, but there is a substantial variation in the results from one anisotropic parameter to another. In particular, it is interesting that the error bars for $\zeta^{(1)}$ and $\zeta^{(2)}$ are much smaller than those for $\zeta^{(3)}$ and the other anisotropic parameters. This is explained by the structure of equations (26)–(28) for the off-diagonal elements W_{12}^{Q}. The expressions for $W_{12}^{S_1}$ and $W_{12}^{S_2}$ have scaling factors $(V_{P0}/V_{S_k})^2$ $(k = 1, 2)$ that reach 4.0 and 6.5 for the model used in our numerical test. Therefore, the elements $W_{12}^{S_k}$ are much more sensitive to $\zeta^{(1)}$ and $\zeta^{(2)}$ than W_{12}^{P} is to $\zeta^{(3)}$, which helps to recover $\zeta^{(1,2)}$ with a higher accuracy.

It may seem that the parameters $\zeta^{(1,2)}$ in Fig. 2 are so well constrained because the S-wave NMO ellipses used for the inversion are noticeably elongated (Fig. 1), and their orientations are well defined. Our next test, however, indicates that the coefficients ζ are extracted in a stable fashion even if the NMO velocity is weakly dependent on azimuth, and the NMO ellipses are close to circles. For the model

in Fig. 3 the ellipticity (i.e., the fractional difference between the semi-major and semi-minor axes of the NMO ellipse) for the P-, S_1-, and S_2-waves reaches only 1.9%, 1.7%, and 2.1%, respectively. Therefore, for all three modes the azimuths β^Q of the semi-major axes are poorly constrained by the data. One may expect that adding a velocity error with a 2% variance (again, we repeated the inversion procedure for 200 realizations of Gaussian noise) can produce significant changes in the orientations of the ellipses and, consequently, sizeable errors in the ζ-coefficients.

However, the error bars for all anisotropic parameters in Fig. 4 are very similar to those in Fig. 2. To explain this result, recall that the angles β^Q themselves are not used in the inversion algorithm which operates with the matrices $\mathbf{W}^Q$ and NMO ellipses. If the ellipses are quasi-circular, their semi-axes become rather sensitive to the off-diagonal element W_{12}^Q, which helps to constrain the coefficients $\zeta^{(1,2,3)}$.

Parameter estimation in layered media

The inversion technique introduced above can be extended to horizontally layered monoclinic media using the generalized Dix equation of Grechka, Tsvankin and Cohen (1999) that yields the exact effective NMO velocity for stratified anisotropic models above a horizontal or dipping reflector. The matrix $\mathbf{W}(L)$ responsible for the effective NMO ellipse from the L-th interface [equation (8)] can be obtained by the following Dix-type averaging of the interval matrices:

$$[\mathbf{W}(L)]^{-1} = \frac{1}{\tau(L)} \sum_{\ell=1}^{L} \tau_\ell \, \mathbf{W}_\ell^{-1} \,, \tag{32}$$

where $\mathbf{W}_\ell$ defines the interval NMO ellipse in layer ℓ and $\tau(L) = \sum_{\ell=1}^{L} \tau_\ell$; τ_ℓ are the interval zero-offset traveltimes. Equation (32) is valid for any anisotropic symmetry and fully accounts for the azimuthal variation of the NMO velocity.

Rewriting equation (32) in the Dix-type differentiation form,

$$\mathbf{W}_\ell^{-1} = \frac{\tau(\ell)\,[\mathbf{W}(\ell)]^{-1} - \tau(\ell-1)\,[\mathbf{W}(\ell-1)]^{-1}}{\tau(\ell) - \tau(\ell-1)} \,, \tag{33}$$

allows one to compute the interval NMO ellipse $\mathbf{W}_\ell$ from the NMO ellipses $\mathbf{W}(\ell-1)$ and $\mathbf{W}(\ell)$ corresponding to the top and bottom of the ℓ-th layer. If the reflector is dipping, application of equation (33) is complicated by the need to compute the matrix $\mathbf{W}(\ell-1)$ (and the interval matrices $\mathbf{W}(\ell)$ in the overburden) for the horizontal slowness components of the oblique zero-offset ray. This problem does not arise for horizontal events considered in this paper because the slowness vector of the zero-offset ray is vertical, and the matrix $\mathbf{W}(\ell-1)$ should be evaluated for the *measured* reflection event from the $(\ell-1)$-th interface.

The interval NMO ellipses can then be inverted for the anisotropic parameters using our single-layer algorithm. The coordinate frame in each layer is defined by the polarization directions of the split shear waves which can be obtained from Alford (1986) rotation of the reflected arrivals followed by polarization layer stripping (Thomsen, Tsvankin and Mueller 1999).

Although Grechka, Tsvankin and Cohen (1999) developed equations (32) and (33) for reflection data, it can also be applied to the NMO ellipses measured in walkaway VSP geometry. Note that the zero-offset reflected ray in laterally homogeneous anisotropic media with a horizontal symmetry plane is always vertical. Therefore, to simulate a reflection experiment, VSP traveltimes should be recorded around a common midpoint located at the projection of the downhole receiver on the surface. Then azimuthally dependent moveout around this CMP location can be used to extract the NMO ellipses and the matrices $\mathbf{W}$ which will be analogous to those for horizontal reflection events.

To test the parameter estimation procedure for stratified monoclinic media, we used a three-layer model with the parameters given in Table 1. According to our convention, the coordinate axes x_1 and x_2 correspond to the polarization directions of the vertically propagating S_1- and S_2-waves, which were the same in all layers. To reproduce a walkaway VSP experiment, we placed three "downhole" receivers at the layer interfaces (the depths are $z = 1.0$, 1.5, and 2.5 km). Using 3-D anisotropic

ray tracing, we computed the traveltimes of the P-, S_1-, and S_2-waves between the receivers and surface sources placed on six differently oriented lines making the angles 0°, 30°, 60°, 90°, 120°, and 150° with the x_1-axis.

The maximum source-receiver offset reaches 1.0 km, which corresponds to a ray-propagation angle of 45° away from the vertical for the most shallow receiver. The traveltimes for this receiver, shown in Fig. 5, substantially vary with azimuth and exhibit strong nonhyperbolic moveout. The simplest way to estimate normal-moveout velocity in the presence of nonhyperbolic moveout, often used in conventional processing, is to mute out far offsets. It is well known (e.g., Alkhalifah and Tsvankin 1995; Grechka and Tsvankin 1999a) that in most cases reflection moveout (especially that of P-waves) is well-represented by a hyperbola up to offsets approximately equal to the reflector depth for reflection data or to one half of the receiver depth for VSP data. Here, however, we choose to preserve the whole moveout curve and correct for nonhyperbolic moveout by applying an equation containing quartic terms in offset. Unlike NMO velocity, the azimuthal variation of the fourth-order moveout term does not have an elliptical form. For a monoclinic layer with a horizontal symmetry plane, this term can be represented by a quartic oval curve that depends on five independent parameters (Sayers and Ebrom 1997). Therefore, the traveltimes of each mode between a given receiver and all sources at the surface were fitted to a quartic moveout equation (Tsvankin and Thomsen 1994) that contains nine free parameters: the vertical traveltime τ_0, three elements of the matrix $\mathbf{W}$ responsible for the NMO ellipse, and five quantities describing the quartic moveout term. Since we were not interested in inverting the azimuthal dependence of nonhyperbolic moveout, we did not use a more elaborate moveout approximation of Tsvankin and Thomsen [1994, equation (30)] that converges at infinitely large offsets. The moveout parameters were obtained by least-squares minimization using the traveltimes at all offsets and azimuths.

The subsequent processing required only four out of nine parameters – the ver-

tical time and the elements of the matrix $\mathbf{W}$. The NMO ellipses obtained from the traveltime data for all three receivers comprise the left column in Fig. 6. The right column displays the interval NMO ellipses determined from the generalized Dix equation (33). Comparison of the two columns in Fig. 6 shows how the changing shape of the effective ellipses translates into the interval ellipse. For example, as the receiver moves from the top to the bottom of the second layer (see Fig. 6a,b), the effective NMO velocity of the S_1-wave (solid line) increases at azimuth 60° and decreases at azimuth 150°. As a result, the interval S_1-ellipse in the second layer is extended at azimuth 60° and squeezed at azimuth 150° (Fig. 6e).

The interval NMO ellipses of the three modes (Fig. 6d–6f), along with the vertical velocities obtained from the vertical times and the exact receiver depths, represent the input data for the parameter estimation procedure described above. The inverted anisotropic parameters listed in Table 2 are quite close to the actual values in Table 1. The maximum error reaches only 0.03 for the two γ coefficients in the second layer. This error, as well as the smaller errors for other anisotropic coefficients, is due to the influence of nonhyperbolic moveout which has not been completely removed by the quartic terms in our moveout equation. Muting out far offsets (or possibly using a more accurate nonhyperbolic moveout equation, see Tsvankin and Thomsen 1994) reduces the errors in the inverted anisotropic parameters to negligible values of less than 0.01.

DISCUSSION AND CONCLUSIONS

Effective monoclinic media with a horizontal symmetry plane represent a general anisotropic model of hydrocarbon reservoirs with two or more vertical fracture systems. An analytic study of normal moveout in monoclinic media, presented here, leads to a Thomsen-style notation that captures the combinations of the stiffness coefficients responsible for the NMO ellipses of P- and S-waves. Natural horizon-

tal coordinate directions for monoclinic models are associated with the orthogonal polarization vectors of the vertically traveling shear waves. The same orientation of the x_1- and x_2-axes is commonly chosen for the higher-symmetry orthorhombic media, where the S-wave polarizations for vertical propagation are confined to the vertical symmetry planes. Hence, aligning the horizontal coordinate axes with the S-wave polarization directions provides a convenient connection between monoclinic and orthorhombic models and allows us to define a set of dimensionless anisotropic parameters by a relatively straightforward extension of Tsvankin's (1997) notation for orthorhombic media. Our parameterization yields concise expressions for the NMO ellipses of horizontal events in a monoclinic layer similar to those obtained by Tsvankin (1997) and Grechka and Tsvankin (1998a) for orthorhombic symmetry. Another advantage of the selected coordinate frame is the reduction in the number of medium parameters from thirteen to twelve.

The anisotropic coefficients of monoclinic media can be separated into two distinctly different groups. The first group contains seven parameters ($\epsilon^{(1,2)}$, $\delta^{(1,2,3)}$, and $\gamma^{(1,2)}$) defined identically to the corresponding Tsvankin's (1997) coefficients in orthorhombic media. While $\delta^{(3)}$ has no influence on the NMO ellipses of P- and S-waves, the remaining six coefficients control the normal-moveout velocities in the coordinate directions x_1 and x_2. The weak-anisotropy approximation for these NMO velocities has the same form as that in the vertical symmetry planes of orthorhombic media. Furthermore, the parameters $\epsilon^{(1,2)}$, $\delta^{(1,2)}$, and $\gamma^{(1,2)}$ are largely responsible for the *semi-axes* of the NMO ellipses of all three modes.

Three additional anisotropic coefficients $\zeta^{(1,2,3)}$ (the second parameter group) depend on the elements of the monoclinic stiffness tensor which vanish in orthorhombic media. Nonzero ζ coefficients cause the *rotation* of the NMO ellipses with respect to the horizontal coordinate axes (i.e., with respect to the shear-wave polarization vectors). In orthorhombic media, $\zeta^{(1,2,3)} = 0$, and the axes of all NMO ellipses coincide with the S-wave polarization directions.

Analytic expressions for the NMO velocities show that the NMO ellipses of the P-, S_1-, and S_2-waves in a horizontal monoclinic layer, combined with the vertical velocities or reflector depth, provide sufficient information for estimating eleven (out of twelve) medium parameters. (The only parameter not constrained by the NMO ellipses of horizontal events is $\delta^{(3)}$.) The first step in the parameter-estimation procedure is to carry out Alford (1986) rotation of short-offset shear-wave data to determine the polarization directions at vertical incidence and establish the coordinate frame for the moveout inversion. Then wide-azimuth 3-D reflection data or multi-azimuth walkaway VSP surveys can be used to reconstruct the NMO ellipses of the waves P, S_1, and S_2. If shear waves are not excited, they can be replaced (in reflection surveys) by the split converted waves PS_1 and PS_2. Although the inversion assumes that all interfaces are horizontal, mild dips under 10° do not cause measurable distortions of NMO ellipses because the NMO velocity for subhorizontal reflectors is approximately governed by the isotropic cosine-of-dip dependence (e.g., Alkhalifah and Tsvankin, 1995).

Our algorithm is designed to invert the exact NMO equations for the anisotropic parameters $\epsilon^{(1,2)}$, $\delta^{(1,2)}$, $\gamma^{(1,2)}$ and $\zeta^{(1,2,3)}$. Although the vertical velocities of the P-wave (V_{P0}) and fast shear wave (V_{S0}) are supposed to be determined directly from the data, we include them in the objective function to improve the fit to the measured NMO ellipses in the presence of noise. Numerical tests on noise-contaminated data indicate that the inversion procedure is sufficiently stable, and all eleven parameters are well constrained by the vertical and NMO velocities.

The most serious restriction of our methodology for reflection data is the assumption that at least one of the vertical velocities (or reflector depth) is known. In general, from reflection moveout alone we can determine only the *ratios* of the vertical velocities of the P- and S-waves. Approximations (26)–(28) show that in this case the NMO ellipses of horizontal events do not contain enough information for estimating the anisotropic parameters. The same conclusion applies to VTI and orthorhom-

bic media (Tsvankin and Thomsen 1995; Grechka, Theophanis and Tsvankin 1999), where certain combination of the anisotropic coefficients (i.e., the "anellipticities" η) can be obtained from dipping events or nonhyperbolic moveout. Similar algorithms can be developed for monoclinic media as well, but the large number of independent parameters may prevent them from being practical. For instance, it can be shown that P-wave NMO velocity from dipping reflectors depends on at least nine parameters, which requires extracting three or more NMO ellipses for different dips and/or azimuths of the reflector.

The moveout-inversion procedure is also based on the assumption that the medium is laterally homogeneous. However, as long as the model is composed of horizontal layers with a horizontal symmetry plane, the influence of weak lateral variation in the elastic constants on the NMO ellipse can be removed using the methodology of Grechka and Tsvankin (1999b). The only information required by their algorithm is the curvature of the zero-offset traveltime surface at the common midpoint that can be estimated directly from surface seismic data.

Using the generalized Dix equation of Grechka, Tsvankin and Cohen (1999), we extended the parameter-estimation procedure to horizontally layered monoclinic media. Alford (1986) rotation and polarization layer-stripping (Thomsen, Tsvankin and Mueller 1999) should be applied prior to the inversion to find depth-varying polarization directions of the vertically propagating shear waves. Although both the Dix differentiation and polarization layer stripping have known limitations with respect to the vertical resolution, they give stable results for coarse intervals with sufficient thickness. The accuracy of our algorithm in evaluating interval anisotropic parameters was verified by inverting ray-traced reflection traveltimes in a three-layer monoclinic model.

ACKNOWLEDGEMENTS

We are grateful to members of the A(nisotropy)-Team of the Center for Wave Phenomena (CWP) at CSM for helpful discussions. Pedro Contreras thanks PDVSA-INTEVEP for giving him the opportunity to work at CWP. V. Grechka and I. Tsvankin acknowledge the support provided by the members of the Consortium Project on Seismic Inverse Methods for Complex Structures at CWP and by the United States Department of Energy (award #DE-FG03-98ER14908). I. Tsvankin was also supported by the Shell Faculty Career Initiation Grant.

APPENDIX A–SELECTION OF THE COORDINATE FRAME

The four-rank elastic stiffness tensor $c_{ijk\ell}^{(\mathrm{mnc})}$ in monoclinic media can be written in the form of the 6×6 matrix $c^{(\mathrm{mnc})}$ [see equation (1)] using the so-called Voigt recipe: $11 \to 1$, $22 \to 2$, $33 \to 3$, $23 \to 4$, $13 \to 5$, and $12 \to 6$. Rotating the tensor $c_{ijk\ell}^{(\mathrm{mnc})}$ by an arbitrary angle θ around the vertical axis x_3 yields a tensor

$$\tilde{c}_{i'j'k'\ell'}^{(\mathrm{mnc})} = c_{ijk\ell}^{(\mathrm{mnc})} r_{i'i} r_{j'j} r_{k'k} r_{\ell'\ell}\,, \tag{A-1}$$

which has the same form as the original tensor $c_{ijk\ell}^{(\mathrm{mnc})}$; summation over repeated indices from 1 to 3 is implied. $r_{m'm}$ in equation (A-1) are components of the rotation matrix defined as

$$\mathbf{r} = \begin{pmatrix} \cos\theta & \sin\theta & 0 \\ -\sin\theta & \cos\theta & 0 \\ 0 & 0 & 1 \end{pmatrix}. \tag{A-2}$$

The rotation of the tensor $\mathbf{c}^{(\mathrm{mnc})}$ by the angle

$$\theta = \frac{1}{2}\,\tan^{-1}\frac{2\,c_{45}}{c_{55} - c_{44}} \tag{A-3}$$

results in $\tilde{c}_{45} = 0$ (Helbig 1994; Mensch and Rasolofosaon 1997; Sayers, 1998). As follows from the Christoffel equation, the horizontal axes in the coordinate frame where $\tilde{c}_{45} = 0$ are parallel to the polarization vectors of the vertically propagating shear waves. Indeed, for vertical propagation (i.e., for the slowness vector $\mathbf{p} = \{0, 0, p_3\}$), the Christoffel equation (2) takes the form:

$$\begin{bmatrix} c_{55}p_3^2 - 1 & c_{45}p_3^2 & 0 \\ c_{45}p_3^2 & c_{44}p_3^2 - 1 & 0 \\ 0 & 0 & c_{33}p_3^2 - 1 \end{bmatrix} \begin{bmatrix} U_1 \\ U_2 \\ U_3 \end{bmatrix} = 0\,. \tag{A-4}$$

The third equation (A-4) describes the vertically polarized P-wave with the slowness

$$q^P \equiv p_3^P = \frac{1}{\sqrt{c_{33}}}\,, \tag{A-5}$$

while the first and the second equations define the slownesses and polarizations of the split shear waves.

Suppose the coordinate frame is rotated around the x_3-axis by the angle θ defined in equation (A-3), so that the coefficient c_{45} in equations (A-4) vanishes. Then this rotation diagonalizes the matrix in equations (A-4):

$$\begin{bmatrix} c_{55}p_3^2 - 1 & 0 & 0 \\ 0 & c_{44}p_3^2 - 1 & 0 \\ 0 & 0 & c_{33}p_3^2 - 1 \end{bmatrix} \begin{bmatrix} U_1 \\ U_2 \\ U_3 \end{bmatrix} = 0\,. \tag{A-6}$$

Evidently, the polarization vectors $\mathbf{U}$, which represent the eigenvectors of equations (A-6), coincide with the horizontal coordinate axes of the new, rotated coordinate frame. Let us choose, for definiteness, the x_1-axis of the rotated coordinate frame to be parallel to the polarization direction of the fast shear wave S_1, while the x_2-axis is parallel to the polarization of the slow wave S_2. Then the slownesses of the S-waves are given by [equation (A-6)]

$$q^{S_1} \equiv p_3^{S_1} = \frac{1}{\sqrt{c_{55}}}\,, \qquad\qquad q^{S_2} \equiv p_3^{S_2} = \frac{1}{\sqrt{c_{44}}}\,. \tag{A-7}$$

Since the S_1-wave travels faster than S_2,

$$q^{S_1} < q^{S_2}\,, \tag{A-8}$$

or

$$c_{55} > c_{44}\,. \tag{A-9}$$

APPENDIX B–EXACT EQUATIONS FOR THE NMO ELLIPSES OF PURE MODES

Equation (13) of the main text can be used to obtain NMO ellipses of any pure (non-converted) modes in a horizontal homogeneous arbitrary anisotropic layer. The vertical slowness components q of the zero-offset ray in a monoclinic layer with the chosen coordinate frame are specified by equations (5). The derivatives $q_{,i} \equiv \partial q/\partial p_i$, and $q_{,ij} \equiv \partial^2 q/\partial p_i \partial p_j$ can be computed directly from the Christoffel equation (2) treated as an implicit relation between the slowness components $F\left(p_1, p_2, q(p_1, p_2)\right) = 0$. Differentiating equation (2) yields (Grechka, Tsvankin and Cohen 1999)

$$q_{,i} = -\frac{F_{p_i}}{F_q}$$

and

$$q_{,ij} = -\frac{F_{p_i p_j} + F_{p_i q} q_{,j} + F_{p_j q} q_{,i} + F_{qq} q_{,i} q_{,j}}{F_q}\,, \tag{B-1}$$

where $F_{p_i} \equiv \partial F/\partial p_i$, $F_q \equiv \partial F/\partial q$, $F_{p_i p_j} \equiv \partial^2 F/\partial p_i \partial p_j$, $F_{p_i q} \equiv \partial^2 F/\partial p_i \partial q$, and $F_{qq} \equiv \partial^2 F/\partial q^2$. All terms in equation (B-1) can be found explicitly from the Christoffel equation (2).

Substituting the vertical slowness components (5) (the horizontal slownesses are equal to zero) and their derivatives (B-1) into the general equation (13), we obtain the following exact expressions for the elements of the matrices $\mathbf{W}^Q$ ($Q = P$, S_1, or S_2) describing the NMO ellipses of the pure modes.

• P-wave:

$$W_{11}^P = \frac{1}{f^P}\left[(c_{33}-c_{55})\left(c_{23}^2 + 2\,c_{23}\,c_{44} + c_{33}\,c_{44}\right) + c_{36}^2\,(c_{33}-c_{44})\right];$$

$$W_{12}^P = -\frac{c_{36}}{f^P}\left[c_{33}\,(c_{44}+c_{55}+c_{13}+c_{23}) - c_{44}\,(c_{55}+c_{13}) - c_{55}\,(c_{44}+c_{23})\right]; \tag{B-2}$$

$$W_{22}^P = \frac{1}{f^P}\left[(c_{33}-c_{44})\left(c_{13}^2 + 2\,c_{13}\,c_{55} + c_{33}\,c_{55}\right) + c_{36}^2\,(c_{33}-c_{55})\right],$$

where

$$
\begin{aligned}
f^P = & \left(c_{13}^2 + c_{33}\, c_{55}\right)\, \left(c_{23}^2 + 2\, c_{23}\, c_{44} + c_{33}\, c_{44}\right) \\
& + 2\, c_{13}\, \left({c_{23}}^2\, c_{55} + c_{44}\, c_{55}\, (c_{33} + 2\, c_{23}) - c_{36}^2\, \left(c_{23} + c_{44}\right)\right) \\
& + c_{36}^2\, \left(c_{33}\, (c_{44} + c_{55}) - 2\, c_{55}\, (2\, c_{44} + c_{23}) + c_{36}^2\right)\, .
\end{aligned}
\tag{B-3}
$$

- S_1-wave:

$$
W_{11}^{S_1} = \frac{c_{66}\, (c_{55} - c_{33}) + c_{36}^2}{f^{S_1}}\, ;
$$

$$
W_{12}^{S_1} = \frac{c_{16}\, (c_{33} - c_{55}) - c_{36}\, (c_{13} + c_{55})}{f^{S_1}}\, ;
\tag{B-4}
$$

$$
W_{22}^{S_1} = \frac{c_{13}^2 + 2\, c_{13}\, c_{55} + c_{55}^2 + c_{11}\, (c_{55} - c_{33})}{f^{S_1}}\, ,
$$

where

$$
f^{S_1} = c_{66}\, (c_{13} + c_{55})^2 + (c_{33} - c_{55})\, \left(c_{16}^2 - c_{11}\, c_{66}\right) - 2\, c_{16}\, c_{36}\, (c_{13} + c_{55}) + c_{11}\, c_{36}^2\, .
\tag{B-5}
$$

- S_2-wave:

$$
W_{11}^{S_2} = \frac{c_{23}^2 + 2\, c_{23}\, c_{44} + c_{44}^2 + c_{22}\, (c_{44} - c_{33})}{f^{S_2}}\, ;
$$

$$
W_{12}^{S_2} = \frac{c_{26}\, (c_{33} - c_{44}) - c_{36}\, (c_{23} + c_{44})}{f^{S_2}}\, ;
\tag{B-6}
$$

$$
W_{22}^{S_2} = \frac{c_{66}\, (c_{44} - c_{33}) + c_{36}^2}{f^{S_2}}\, ,
$$

where

$$
f^{S_2} = c_{66}\, (c_{23} + c_{44})^2 + (c_{33} - c_{44})\, \left(c_{26}^2 - c_{22}\, c_{66}\right) - 2\, c_{26}\, c_{36}\, (c_{23} + c_{44}) + c_{22}\, c_{36}^2\, .
\tag{B-7}
$$

REFERENCES

Alford R.M. 1986. Shear data in the presence of azimuthal anisotropy. 56th SEG meeting, Expanded Abstracts, 476–479.

Alkhalifah T. and Tsvankin I. 1995. Velocity analysis in transversely isotropic media. *Geophysics* **60**, 1550–1566.

Bakulin A., Grechka V. and Tsvankin, I. 1999. Estimation of fracture parameters from reflection seismic data. Part III: Fractures producing effective monoclinic media. *Geophysics*, submitted.

Corrigan D., Withers R., Darnall J. and Skopinski T. 1996. Fracture mapping from azimuthal velocity analysis using 3D surface seismic data. 66th SEG Meeting, Denver, Expanded Abstracts, 1834–1837.

Fedorov F.I. 1968. *Theory of elastic waves in crystals*. Plenum Press.

Grechka V., Theophanis S. and Tsvankin I. 1999. Joint inversion of P- and PS-waves in orthorhombic media: Theory and a physical-modeling study. *Geophysics* **64**, 146–161.

Grechka V. and Tsvankin I. 1998a. 3-D description of normal moveout in anisotropic media. *Geophysics* **63**, 1079–1092.

Grechka V. and Tsvankin I. 1998b. Inversion of azimuthally dependent NMO velocity in transversely isotropic media with a tilted axis of symmetry. 68th SEG meeting, New Orleans, Expanded Abstracts, 1483–1486.

Grechka V. and Tsvankin I. 1999a. 3-D moveout velocity analysis and parameter estimation for orthorhombic media: *Geophysics* **64**, 820–837.

Grechka V. and Tsvankin I. 1999b. 3-D moveout inversion in azimuthally anisotropic media with lateral velocity variation: Theory and a case study. *Geophysics* **64**, 1202–1218.

Grechka V., Tsvankin I. and Cohen J.K. 1999. Generalized Dix equation and analytic treatment of normal-moveout velocity for anisotropic media. *Geophysical Prospecting* **47**, 117–148.

Helbig K. 1994. *Foundations of anisotropy for exploration seismics: Handbook of Geophysical Exploration* (eds. Helbig K. and Treitel S.). **22**, Pergamon Press.

Mensch T. and Rasolofosaon P. 1997. Elastic-wave velocities in anisotropic media of arbitrary symmetry – generalization of Thomsen's parameters ϵ, δ, and γ. *Geophysical Journal International* **128**, 43–64.

Musgrave M.J.P. 1970. *Crystal acoustics*. Holden Day.

Pérez M.A., Grechka V. and Michelena R.J. 1999. Fracture detection in a carbonate reservoir using a variety of seismic methods. *Geophysics* **64**, 1266–1276.

Press W.H., Flannery B.P., Teukolsky S.A. and Vetterling W.T. 1987. *Numerical recipes: the art of scientific computing*. Cambridge University Press.

Pšenčík I. and Gajewski D. 1998. Polarization, phase velocity and NMO velocity of qP-waves in arbitrary weakly anisotropic media. *Geophysics* **63**, 1754–1766.

Sayers C.M. 1998. Misalignment of the orientation of fractures and the principal axes for P and S-waves in rocks containing multiple non-orthogonal fracture sets. *Geophysical Journal International* **133**, 459–466.

Sayers C.M. and Ebrom D.A. 1997. Seismic traveltime analysis for azimuthally anisotropic media: Theory and experiment. *Geophysics* **62**, 1570–1582.

Schoenberg M. and Sayers C. 1995. Seismic anisotropy of fractured rock. *Geophysics* **60**, 204–211.

Thomsen L. 1986. Weak elastic anisotropy. *Geophysics* **51**, 1954–1966.

Thomsen L., Tsvankin I. and Mueller M.C. 1999. Coarse-layer stripping of vertically variable azimuthal anisotropy from shear-wave data. *Geophysics* **64**, 1126-1138.

Tsvankin I. 1997. Anisotropic parameters and P-wave velocity for orthorhombic media. *Geophysics* **62**, 1292–1309.

Tsvankin I. and Thomsen L. 1994. Nonhyperbolic reflection moveout in anisotropic media. *Geophysics* **59**, 1290–1304.

Tsvankin I. and Thomsen L. 1995. Inversion of reflection traveltimes for transverse isotropy. *Geophysics* **60**, 1095–1107.

Winterstein D.F. and Meadows M.A. 1991. Shear-wave polarizations and subsurface stress directions at Lost Hills field. *Geophysics* **56**, 1331–1348.

FIGURES

FIG. 1. Exact (solid) and approximate (dotted) NMO ellipses in a monoclinic layer with the following parameters: $V_{P0} = 2.0$ km/s, $V_{S0} = 1.0$ km/s, $\epsilon^{(1)} = 0.3$, $\epsilon^{(2)} = 0.4$, $\delta^{(1)} = 0.2$, $\delta^{(2)} = 0.25$, $\gamma^{(1)} = -0.1$, $\gamma^{(2)} = 0.15$, $\zeta^{(1)} = -0.03$, $\zeta^{(2)} = -0.02$, $\zeta^{(3)} = 0.04$.

FIG. 2. Results of the moveout inversion for a monoclinic layer with the vertical velocities and the parameter vector $\boldsymbol{\chi} \equiv [\epsilon^{(1)}, \epsilon^{(2)}, \delta^{(1)}, \delta^{(2)}, \gamma^{(1)}, \gamma^{(2)}, \zeta^{(1)}, \zeta^{(2)}, \zeta^{(3)}]$ for the model from Fig. 1 . The dots represent the exact values of the anisotropic parameters, the bars mark the $\pm$ standard deviation in each parameter. The standard deviations in the velocities V_{P0} and V_{S0} (not shown here) are 2.1% and 2.0%, respectively.

FIG. 3. Exact NMO ellipses in a monoclinic layer with the parameters $V_{P0} = 2.0$ km/s, $V_{S0} = 1.0$ km/s, $\epsilon^{(1)} = 0.123$, $\epsilon^{(2)} = 0.075$, $\delta^{(1)} = \delta^{(2)} = 0.1$, $\gamma^{(1)} = -0.1$, $\gamma^{(2)} = 0.15$, $\zeta^{(1)} = -0.002$, $\zeta^{(2)} = -0.003$, $\zeta^{(3)} = 0.02$.

FIG. 4. Results of the moveout inversion for a monoclinic layer with the parameters from Fig. 3 . The dots represent the exact values of the anisotropic parameters, the bars mark the $\pm$ standard deviation in each parameter. The standard deviations in the velocities V_{P0} and V_{S0} are equal to 2.0%.

FIG. 5. Squared traveltimes of the direct P-, S_1-, and S_2-waves excited at the surface and recorded by a "downhole" receiver at a depth of 1.0 km. Each symbol corresponds to a fixed source-receiver azimuth, as indicated in the upper-left corner of the plot.

FIG. 6. (a), (b), (c) NMO ellipses determined from ray-traced traveltimes for the

downhole receivers at depths $z = 1.0$, 1.5, and 2.5 km, respectively. (d), (e), (f) Interval NMO ellipses computed for the first (subsurface), second and third layer using the generalized Dix equation (33). Dotted ellipses correspond to the P-wave, solid – to the S_1-wave, and dashed – to the S_2-wave.

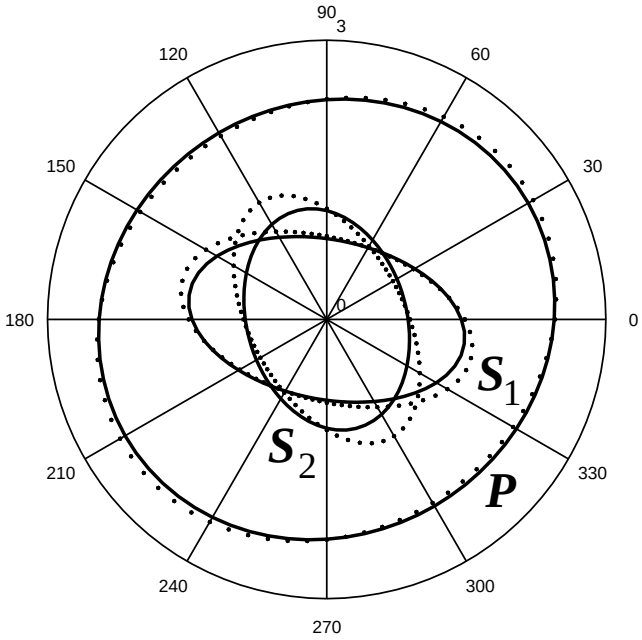

FIG. 1. Exact (solid) and approximate (dotted) NMO ellipses in a monoclinic layer with the following parameters: $V_{P0} = 2.0$ km/s, $V_{S0} = 1.0$ km/s, $\epsilon^{(1)} = 0.3$, $\epsilon^{(2)} = 0.4$, $\delta^{(1)} = 0.2$, $\delta^{(2)} = 0.25$, $\gamma^{(1)} = -0.1$, $\gamma^{(2)} = 0.15$, $\zeta^{(1)} = -0.03$, $\zeta^{(2)} = -0.02$, $\zeta^{(3)} = 0.04$.

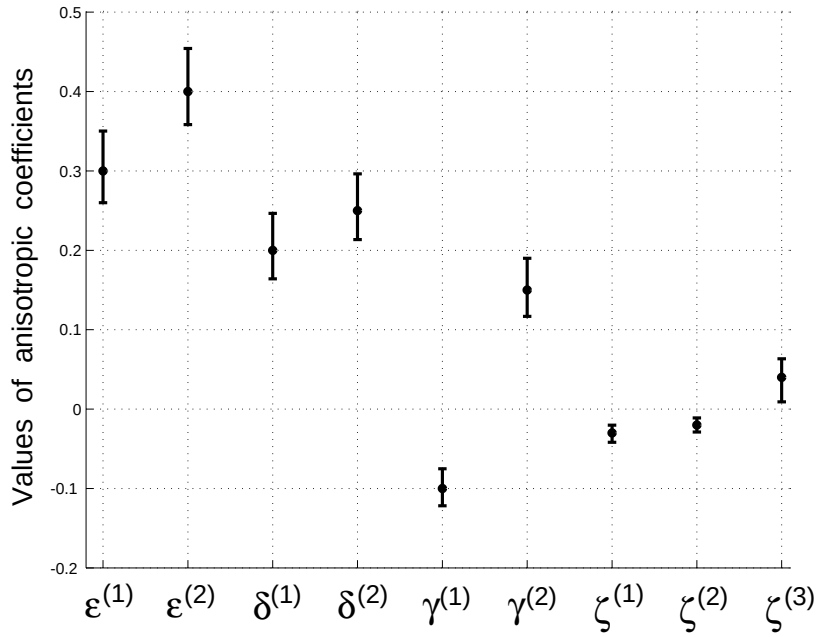

FIG. 2. Results of the moveout inversion for a monoclinic layer with the vertical velocities and the parameter vector $\boldsymbol{\chi} \equiv [\epsilon^{(1)}, \epsilon^{(2)}, \delta^{(1)}, \delta^{(2)}, \gamma^{(1)}, \gamma^{(2)}, \zeta^{(1)}, \zeta^{(2)}, \zeta^{(3)}]$ for the model from Fig. 1. The dots represent the exact values of the anisotropic parameters, the bars mark the $\pm$ standard deviation in each parameter. The standard deviations in the velocities V_{P0} and V_{S0} (not shown here) are 2.1% and 2.0%, respectively.

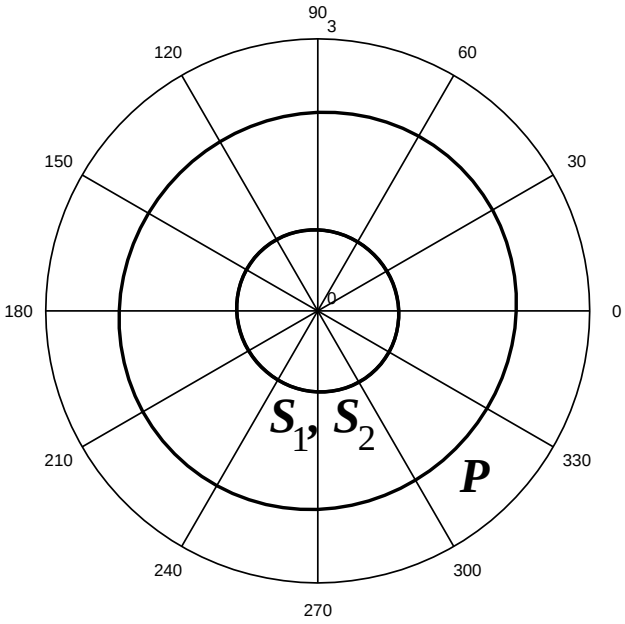

FIG. 3. Exact NMO ellipses in a monoclinic layer with the parameters $V_{P0} = 2.0$ km/s, $V_{S0} = 1.0$ km/s, $\epsilon^{(1)} = 0.123$, $\epsilon^{(2)} = 0.075$, $\delta^{(1)} = \delta^{(2)} = 0.1$, $\gamma^{(1)} = -0.1$, $\gamma^{(2)} = 0.15$, $\zeta^{(1)} = -0.002$, $\zeta^{(2)} = -0.003$, $\zeta^{(3)} = 0.02$.

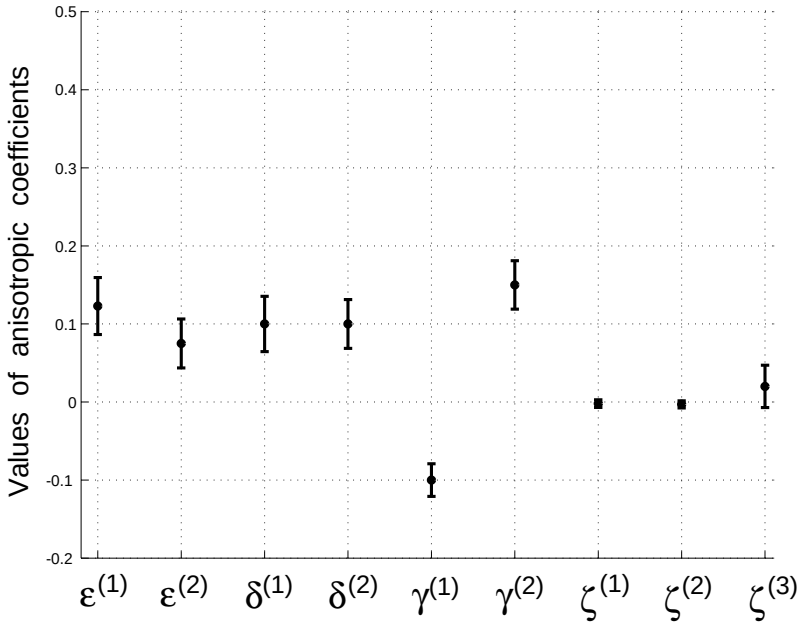

FIG. 4. Results of the moveout inversion for a monoclinic layer with the parameters from Fig. 3. The dots represent the exact values of the anisotropic parameters, the bars mark the ± standard deviation in each parameter. The standard deviations in the velocities V_{P0} and V_{S0} are equal to 2.0%.

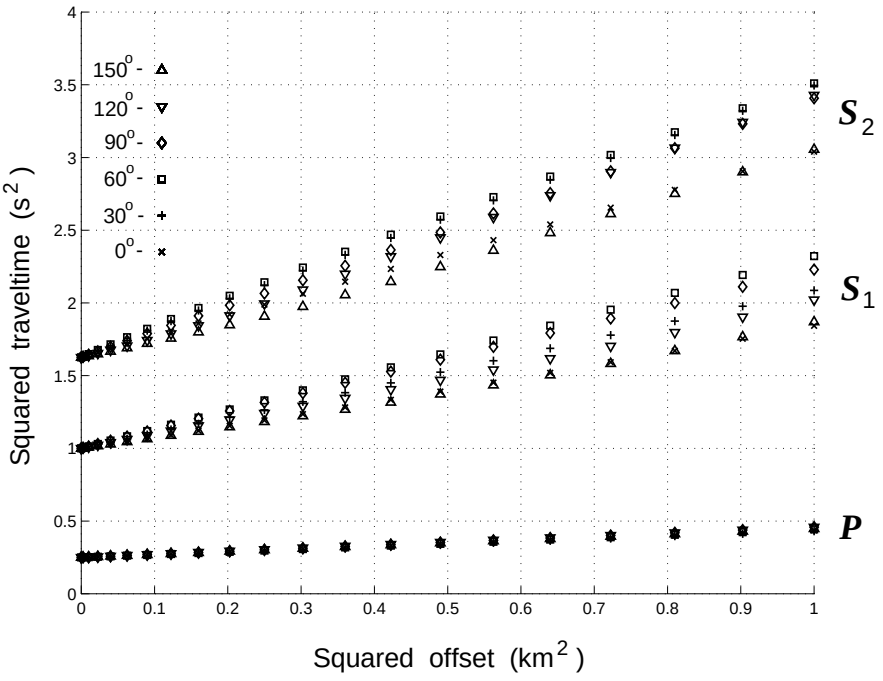

FIG. 5. Squared traveltimes of the direct P-, S_1-, and S_2-waves excited at the surface and recorded by a "downhole" receiver at a depth of 1.0 km. Each symbol corresponds to a fixed source-receiver azimuth, as indicated in the upper-left corner of the plot.

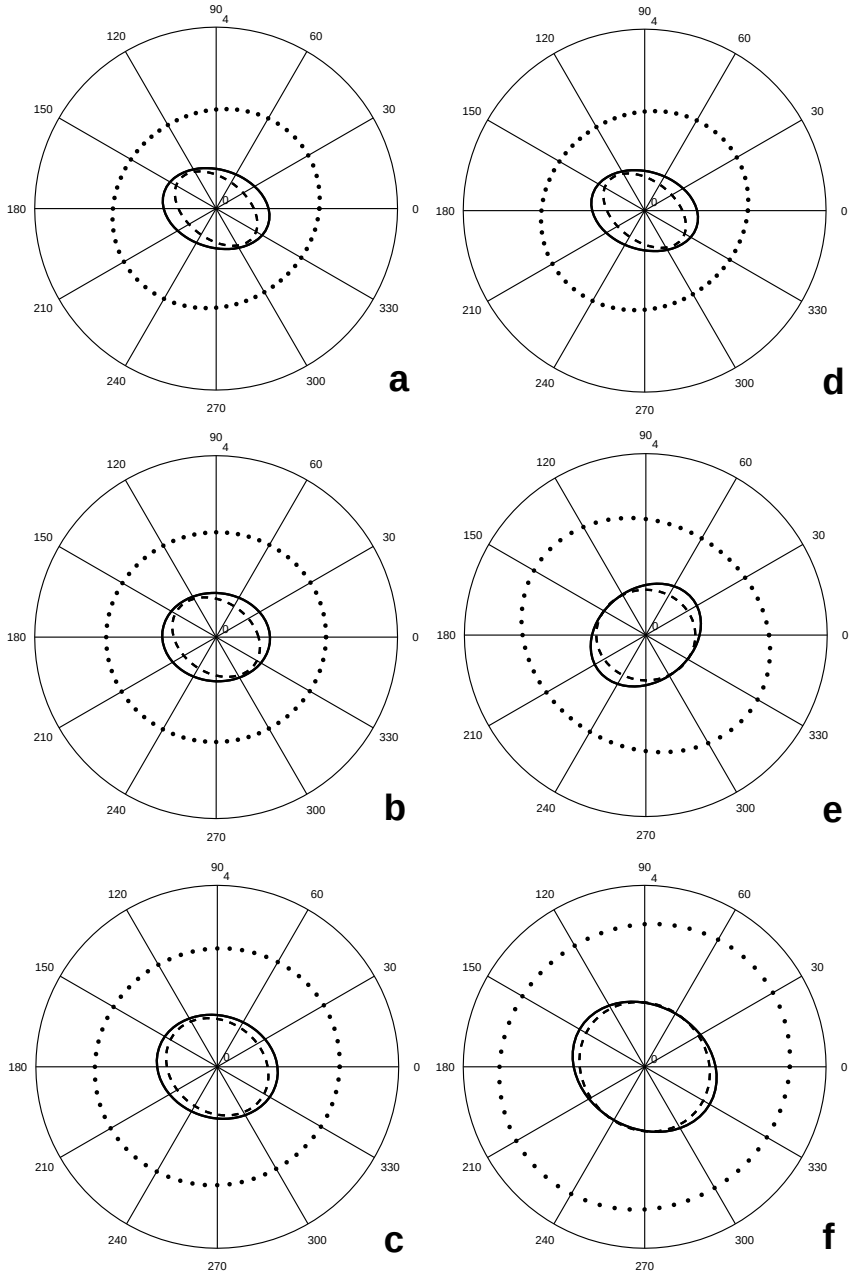

FIG. 6. (a), (b), (c) NMO ellipses determined from ray-traced traveltimes for the down-hole receivers at depths $z = 1.0$, 1.5, and 2.5 km, respectively. (d), (e), (f) Interval NMO ellipses computed for the first (subsurface), second and third layer using the generalized Dix equation (33). Dotted ellipses correspond to the P-wave, solid – to the S_1-wave, and dashed – to the S_2-wave.